New Journal of Physics

Attosecond metrology in the few-optical-cycle regime

G Sansone, E Benedetti, C Vozzi, S Stagira and M Nisoli[1]

National Laboratory for Ultrafast and Ultraintense Optical Science,
CNR–INFM, Department of Physics, Politecnico di Milano,
Piazza Leonardo da Vinci 32, 20133 Milano, Italy
E-mail: mauro.nisoli@fisi.polimi.it

Abstract. The polarization gating method in combination with few-optical-cycle driving pulses with controlled waveform is a powerful technique for the generation of isolated few-cycle attosecond pulses. We show that such a technique allows one to generate attosecond pulses tunable in a broad spectral region, corresponding to more than 26 eV. Complete temporal characterization of the attosecond pulses has been obtained by using the frequency resolved optical gating for complete reconstruction of attosecond bursts technique. The physical processes which determine the temporal confinement of the extreme ultraviolet radiation and the effects of various experimental parameters on the electric field of the attosecond pulses have been investigated using numerical simulations based on the nonadiabatic saddle-point method.

[1] Author to whom any correspondence should be addressed.

Contents

1. Introduction

In the last few years dramatic progress has been achieved in the field of attosecond technology, mainly due to breakthroughs in laser science and to the introduction of new techniques for temporal characterization of extreme ultraviolet (XUV) attosecond pulses, produced by high-order harmonic generation (HHG) in noble gases. Attosecond science is now a well-established research field, which promises to offer formidable tools for the investigation and control of fundamental atomic and subatomic electron processes [1, 2]. Novel experimental approaches have been proposed and partly implemented in order to achieve time-resolved imaging of electronic and molecular structures. In this context, the exploitation of the recollision physics, in combination with optical science, offers the possibility to observe, with sub-Angstrom resolution, atomic and molecular orbitals [3, 4].

Important achievements have been obtained in the generation of attosecond pulses, in the form of trains of pulses [5] or isolated pulses. A train of almost Fourier-transform-limited 170 as pulses has been produced by amplitude and phase control of ten consecutive plateau harmonics generated in argon, thus demonstrating optical manipulation on attosecond timescale [6]. More recently, trains of 130 as pulses have been obtained by harmonic generation in neon and dispersion compensation with a Zr filter [7]. In the case of isolated attosecond pulses, two generating schemes have been proposed and implemented. The first scheme is based on the use of few-cycle (duration <6 fs) driving pulses with stabilized carrier-envelope phase (CEP) and spectral selection of the cutoff portion of the harmonic spectrum [8, 9]: pulses as short as 250 as were generated using this method in 2004 [10]. The minimum pulse duration of the XUV pulses is limited by the bandwidth of the selected cutoff harmonics. A different approach is based on the use of phase-stabilized few-cycle driving pulses in combination with the polarization gating technique [11, 12], which exploits the strong dependence of the harmonic generation process on the ellipticity of the driving pulses in order to obtain a temporal window of linear polarization for the fundamental pulses. XUV generation is possible only during this temporal polarization gate, which can be shorter than half an optical cycle of the fundamental radiation [13]. Isolated pulses with duration down to 130 as around 36 eV photon energy, which consist of less than 1.2 periods of the central frequency, were generated by the authors in 2006 [14].

In this work, we demonstrate that the polarization gating method with few-cycle phase-stabilized driving pulses allows one to tune, on a very broad spectral region, broadband XUV radiation corresponding to isolated attosecond pulses. The XUV pulses have been temporally characterized using the frequency resolved optical gating for complete reconstruction of attosecond bursts (FROG CRAB) technique [15]. The experimental results have been analyzed using the nonadiabatic saddle-point (NASP) method [16, 17], whose results turn out to be in excellent agreement with the measurements.

The paper is organized as follows. In section 2, we experimentally demonstrate the generation of isolated attosecond pulses tunable in a broad spectral region. In section 3 the NASP method is used to obtain a clear physical picture of the effects of the CEP of the driving pulses on the temporal confinement characteristics of the polarization gating method. In particular a simple interpretation of the transition between the emission of an isolated pulse and a pair of pulses upon changing the CEP of the driving pulses will be discussed. Section 4 is devoted to attosecond metrology: after a brief theoretical introduction of the FROG CRAB technique, experimental results are shown and analyzed. The effects on the electric field of the attosecond pulses of various experimental parameters characterizing the driving pulses, namely CEP, intensity and duration fluctuations, will be analyzed in section 5, in the framework of the NASP method. Finally, section 6 contains the conclusions.

2. Tunable isolated attosecond pulses by phase-stabilized polarization gating

Polarization shaping of an infrared (IR) pulse in the temporal domain can be achieved by using two birefringent plates [12]. In our experimental condition, the first plate is a $181\,\mu$m thick multiple-order plate, which splits the 5 fs linearly polarized input pulse into two orthogonally polarized pulses delayed by 5.8 fs. The second one is a zero-order quarter waveplate. After the two plates the pulse is linearly polarized around the center and circularly or elliptically polarized on the leading and trailing edges. In this way it is possible to create a linear polarization gate shorter than one-half the optical cycle of the driving IR field, thus giving rise to the generation of isolated attosecond pulses. We note that the gate position is imposed by the intensity profile of the pulse while the emission time is linked to the CEP of the electric field. It has been demonstrated that upon changing the CEP of the driving pulses it is possible to generate either one or two XUV pulses [13].

25 fs pulses generated by a Ti:sapphire laser system (0.7 mJ energy, 1 kHz repetition rate) have been injected into a 60 cm long hollow fiber [18] with inner diameter of 0.5 mm at the entrance side and 0.3 mm at the exit side, filled with argon at a pressure of about 0.25 bar in order to achieve a pulse duration <6 fs after recompression using ultrabroadband chirped mirrors. The CEP of the IR pulses has been actively stabilized as described in [19]. The pulses used for the experiments present an overall CEP residual fluctuation of $\sim$90 mrad (rms) [20]. The CEP can be finely adjusted by introducing into the beam path a glass plate with variable thickness; we have used a pair of wedges mounted on a stepper motor. The XUV radiation has been generated by focusing the IR pulses on a 3.5 mm thick gas cell with static pressure. The additional positive dispersion introduced by the two plates used for polarization gating was precompensated by the chirped mirrors.

We have first adjusted the CEP of the IR pulses in order to generate broadband and continuous XUV spectra, both in argon and in neon. Upon changing the CEP of the driving pulses a clear transition from two to a single emission burst was observed in the spectral domain
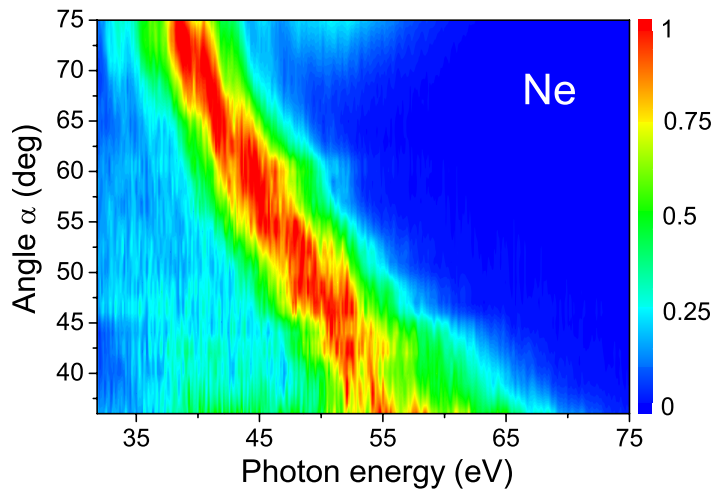
Figure 1. XUV spectra measured in neon for different values of the angle α between the electric field of the linearly polarized input pulse and the neutral axis of the first multiple-order waveplate. The CEP of the driving 5 fs pulses has been fixed in order to generate continuous XUV spectra.

in both gases. We have then changed the angle α between the electric field of the linearly polarized input pulse and the neutral axis of the first multiple-order waveplate (the initial α value was 45°). Figure 1 shows a series of 40 XUV spectra measured in neon in correspondence to different values of the angle α. Each horizontal line represents a spectrum measured at a fixed waveplate angle. It is evident that the XUV radiation can be continuously and finely tuned in a broad spectral region by rotating the multiple-order waveplate: the maximum spectral shift is ∼20 eV. It is worth pointing out that the generated XUV spectra are continuous over all the recorded bandwidth (thus corresponding to a single emission process) for all the values of α shown in figure 1, in the range ∼35° < α <∼ 75°. The transform limited duration of the generated chirped pulses is <130 as: this is the temporal resolution that could be achieved in measurements performed with electron wavepackets generated by such attosecond pulses [21]. A further increase of α determines an increase of the width of the polarization gate, which gives rise to the generation of modulated spectra, corresponding to two emission bursts. Therefore, while the thickness of the multiple-order plate, which determines the temporal delay between the two perpendicularly polarized pulses at the input of the second plate, must be precisely fixed on the basis of the driving pulse duration, the confinement of the XUV generation to a single attosecond pulse is not very sensitive to the alignment of the plate axis with respect to the polarization direction of the input pulses. By varying the value of α, it is possible to finely change the time dependence of the polarization of the IR field and therefore the electron trajectories. In this way the energy of the electron wavepacket recolliding with the parent ion can be tuned determining the emission of tunable XUV pulses.

Figure 2 shows a series of 40 XUV spectra generated in argon using the same driving pulses and varying the angle α. Also in this case, the XUV radiation is continuous over all the recorded bandwidth and can be continuously tuned in a more restricted spectral region, with respect to the case of neon: the maximum spectral shift is ∼6.5 eV. Therefore, by considering both gases, it is possible to achieve a complete tunability over more than 26 eV; indeed, as
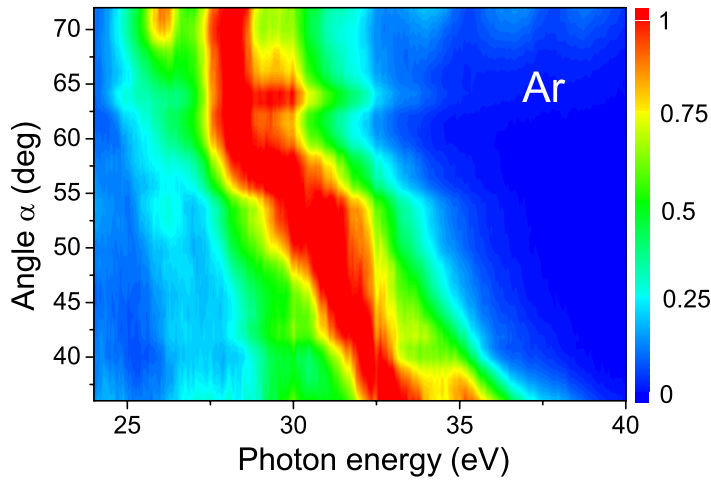
Figure 2. XUV spectra measured in argon for different values of the angle α. The CEP of the driving 5 fs pulses has been fixed in order to generate continuous XUV spectra.

shown in figures 1 and 2, the spectral position of the XUV spectrum generated in neon in correspondence to $\alpha = 75°$ is very close in frequency to that of the spectrum generated in argon in correspondence to $\alpha = 35°$.

Before proceeding with discussion of the experimental technique used for complete temporal characterization of isolated attosecond pulses, we will investigate the physical processes leading to the confinement of the XUV radiation obtained by the polarization gating technique with phase-stabilized few-cycle driving pulses using a numerical model based on the NASP method [16, 17].

3. NASP simulations: electron trajectories and polarization state of attosecond pulses

Using the saddle-point method, the Fourier transform of the dipole moment, $d(\omega)$, can be written as a coherent superposition of the contributions from the electron quantum paths corresponding to the complex saddle-point solutions $(\mathbf{p}_s, t_s, t'_s)$, where: $\mathbf{p}_s$ is the stationary value of the momentum acquired by an electron which is set free at time t'_s and recombines with the parent ion at time t_s. The sum over the relevant quantum paths can be decomposed into two terms related to the short and long quantum paths. In the following, we will assume an initial driving IR field propagating in the z-direction, linearly polarized along the x-direction. The dipole moment generated by the IR pulse, after the modulation of its polarization state, can be decomposed into two components, $d_x(\omega)$ and $d_y(\omega)$, along the orthogonal directions x and y, respectively:

$$d_x(\omega) = \sum_s |d_{x_s}(\omega)| \exp[i\Phi_{xs}(\omega)],$$

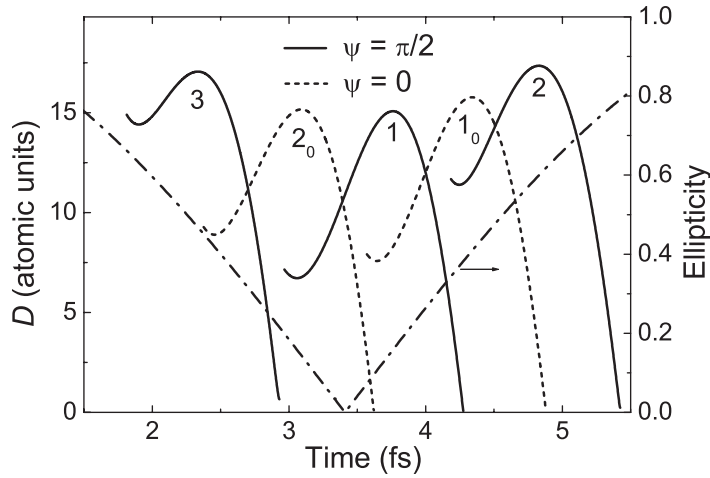$$d_y(\omega) = \sum_s |d_{y_s}(\omega)| \exp[i\Phi_{ys}(\omega)],$$

(1)

Figure 3. Electron distance $D(t)$, for a few quantum paths, calculated assuming 5 fs driving pulses with shaped polarization and two different CEP values. The dash-dotted curve is the ellipticity of the IR pulse.

where the sums are performed over the solutions $(\mathbf{p}_s, t_s, t_s')$ of the saddle-point equations and take into account the contributions of the relevant short quantum paths. Indeed, in the experiments, we have selected the contribution of the short paths by placing the gas cell after the laser focus [22]. Φ_{xs} and Φ_{ys} are the phases of the complex functions $d_{x_s}(\omega)$ and $d_{y_s}(\omega)$, respectively. The spectral intensity can be calculated as $I(\omega) = |d_x(\omega)|^2 + |d_y(\omega)|^2$. The electron trajectories can be described by the following equation [23, 24]:

$$\mathbf{r}(t) = x_s(t)\hat{\mathbf{e}}_x + y_s(t)\hat{\mathbf{e}}_y = \mathbf{p}_s \cdot (t - t_s') + \int_{t_s'}^{t} \mathbf{A}(t'')dt'',\qquad(2)$$

where t is the real time, $\mathrm{Re}(t_s') \leqslant t \leqslant \mathrm{Re}(t_s)$. The real parts of $x_s(t)$ and $y_s(t)$ are related to the actual electron trajectory in space and time, which can be visualized considering the temporal evolution of the distance, $D(t)$, of the electron from the origin $\mathbf{r} = 0$, $D^2(t) = \mathrm{Re}(x_s)^2 + \mathrm{Re}(y_s)^2$. Figure 3 shows the electron distance $D(t)$, for a few quantum paths, calculated in the case of XUV radiation produced in argon by 5 fs driving pulses with time-dependent polarization, for two different CEP values. While $D(t_s) = 0$, both $D(\mathrm{Re}(t_s'))$ and $D(\mathrm{Re}(t_s))$ are nonzero [23]. In agreement with the well accepted picture, harmonic emission is possible only when the electron wavepacket is driven back to recollide with the parent ion $D(\mathrm{Re}(t_s)) \approx 0$, whereas $D(\mathrm{Re}(t_s'))$, which can be interpreted as the electron position at the end of the tunnel, is of the order of a few atomic units. We note that the XUV emission rate associated with each quantum path is inversely proportional to the initial electron distance from the origin: the larger $D(\mathrm{Re}(t_s'))$ is, the lower is the corresponding contribution to the overall emission. On the basis of the previous observations, figure 3 offers a clear physical interpretation of the transition between the emission of an isolated pulse and a pair of pulses, upon changing the CEP of the IR field. When $\psi = \pi/2$ (solid curves in figure 3) a single quantum path (path 1) gives the most relevant contribution to the XUV emission. Indeed, such a path is characterized by an electron position at the end of tunnel much closer to the origin than the other two adjacent paths (paths 2 and 3 in figure 3). In contrast, when $\psi = 0$ (dashed curves in figure 3) two paths give comparable contributions, so that two attosecond pulses are emitted. Therefore, the CEP stabilization of the driving pulses is a crucial prerequisite for reliable generation of isolated attosecond pulses.
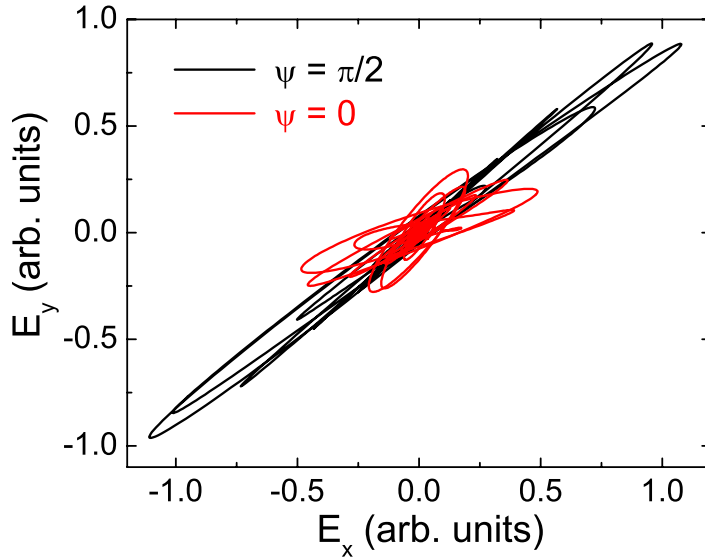
Figure 4. Electric field evolution of the XUV pulses calculated using the NASP method for two CEP values of the driving field and the same parameters used for the simulations reported in figure 3. E_x and E_y are the components of the XUV electric field along the x- and y-axes, respectively.

We have then investigated the temporal evolution of the polarization state of the attosecond pulses as a function of the CEP of the driving field. The results of the numerical simulations, performed using the same parameters used for the previous calculations, are shown in figure 4, where the electric field evolution for two CEP values is reported. E_x and E_y are the components of the XUV electric field along the x- and y-axes, respectively. We note that, when two attosecond pulses are generated ($\psi = 0$), the orientation of the major polarization axis is different for the two pulses.

4. Temporal characterization of attosecond pulses

4.1. FROG CRAB

Complete temporal characterization of the attosecond pulses has been obtained using the technique of FROG CRAB (hereafter called CRAB) [15]. The XUV attosecond pulse ionizes a gas, by single photon absorption, thus generating an attosecond electron pulse, which, far from any resonance, is a perfect replica of the optical pulse. The conversion of the XUV pulse into an electron wavepacket is obtained in the presence of a streaking IR pulse, whose electric field acts as an ultrafast phase modulator on the generated electron wavepacket. In this way, a time-nonstationary filter [25], which is required to achieve the temporal characterization of the ultrashort pulse, is realized. The evolution of the photo-ionization spectra as a function of the delay, τ, between the attosecond and the IR pulses (hereafter called CRAB trace) allows one to retrieve the temporal intensity profile and phase of the XUV pulses and the electric field of the IR pulse. The photo-ionization spectrum is given by [15, 16, 26]

$$S(W, \tau) = \left| \int_{-\infty}^{\infty} \mathrm{d}t \, \mathrm{e}^{\mathrm{i}\phi(t)} \mathbf{d} \cdot \mathbf{E}_X(t - \tau) \, \mathrm{e}^{\mathrm{i}(W + I_\mathrm{p})t} \right|^2, \tag{3}$$
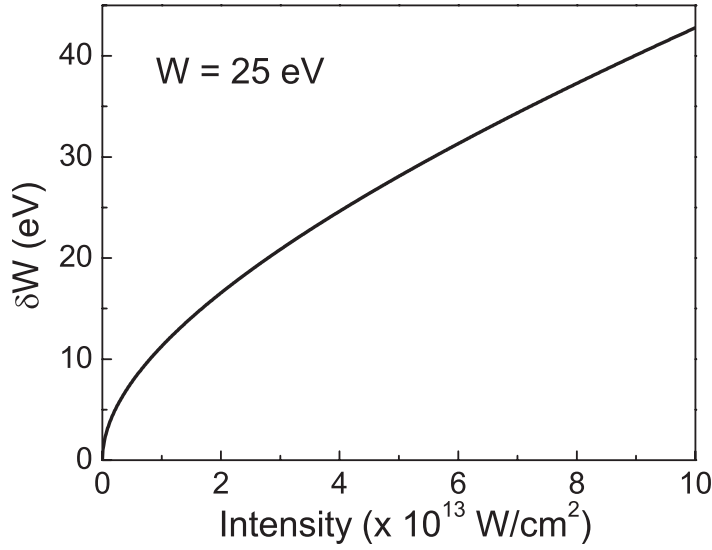
Figure 5. Bandwidth of the electron phase modulator as a function of the intensity of the streaking IR field in the case of electrons with kinetic energy $W = 25\,\text{eV}$ and $\theta = 0$.

where: $\mathbf{E}_X(t)$ is the electric field of the XUV pulse; $\mathbf{d}$ is the dipole transition matrix element from the ground state to the continuum state; W is the final kinetic energy of the electron; I_p is the gas ionization potential and $\phi(t)$ is the temporal phase modulation imposed by the IR streaking pulse to the electron wavepacket, $\mathbf{d} \cdot \mathbf{E}_X(t)$, generated by the attosecond pulse in the continuum. Such phase modulation is given by

$$\phi(t) = -\int_t^\infty dt'[\mathbf{v} \cdot \mathbf{A}(t') + \mathbf{A}^2(t')/2], \tag{4}$$

where $\mathbf{A}(t)$ is the vector potential of the IR field and $\mathbf{v}$ is the final electron velocity. Assuming a linearly polarized streaking IR field $\mathbf{E}_\text{s}(t) = \mathbf{E_0}(t)\cos(\omega_\text{s}t)$, the induced phase modulation is given by $\phi(t) = \phi_1(t) + \phi_2(t) + \phi_3(t)$ [15]

$$\phi_1(t) = -\int_t^\infty dt' U_\text{p}(t'),$$

$$\phi_2(t) = \left(\sqrt{8WU_\text{p}}/\omega_\text{s}\right) \cos\theta \, \cos\omega_\text{s}t, \tag{5}$$

$$\phi_3(t) = -(U_\text{p}/2\omega_\text{s})\sin(2\omega_\text{s}t),$$

where $U_\text{p} = E_0^2(t)/4\omega_\text{s}^2$ is the ponderomotive energy and θ is the angle between $\mathbf{v}$ and the IR polarization direction.

In order to warrant a correct characterization of the electron wavepacket generated by the XUV pulses, the phase modulation imposed by the streaking pulse must be fast enough. The bandwidth of the phase-modulator is given by the maximum value of $|\partial\phi/\partial t|$, which corresponds to the maximum energy shift of the photoelectron spectrum produced by the streaking field [27]. Figure 5 shows the calculated bandwidth, $\delta W = |\partial\phi/\partial t|_\text{max}$, as a function of the streaking pulse intensity in the case of $W = 25\,\text{eV}$ and $\theta = 0$. For a correct XUV pulse
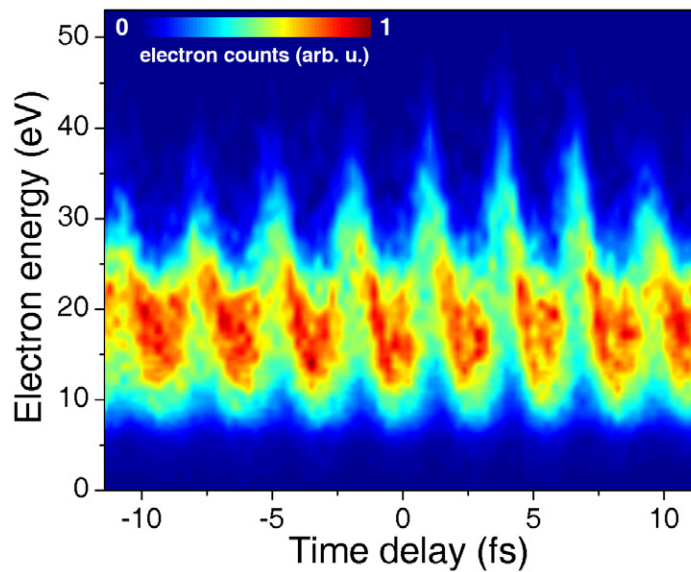
Figure 6. Complete experimental CRAB trace measured as a function of the temporal delay between the attosecond and the streaking IR pulses. Isolated attosecond pulses were generated by phase-stabilized, 5 fs pulses with modulated polarization state. A 100 nm thick aluminium foil has been used to block the fundamental radiation in the XUV beam path.

reconstruction, such bandwidth should be a significant fraction of that of the attosecond field to be characterized.

4.2. Generation and characterization of few-cycle isolated attosecond pulses: experimental results

The laser beam has been spatially separated into two parts using a drilled mirror (5 mm diameter central hole). The inner part passes through two birefringent plates to produce the required modulation of the polarization state and is focused into the argon gas cell. The XUV beam passes through an aluminium filter and is focused in an argon jet by a toroidal mirror. The outer annular part of the IR beam is focused on to the argon jet. The XUV and IR beams are directed on to the argon jet using a collinear geometry. The delay between the XUV attosecond pulses and the streaking IR pulses is controlled by a piezoelectric translator with 1 nm resolution. The photoelectrons generated by single-photon absorption of the XUV pulses were collected within an acceptance angle of $\pm 2°$, around $\theta = 0$, where θ is the angle between the electron velocity and the polarization direction of the IR field.

Figure 6 shows the evolution of the photoelectron spectrum as a function of the temporal delay between the XUV and the streaking IR pulses. The ~ 15 eV energy streaking, which represents the bandwidth of the electron phase modulator, is comparable to the photoelectron bandwidth, therefore the phase modulation imposed by the IR field is fast enough to warrant a correct characterization of the electron wavepacket generated by the attosecond pulse. The periodic oscillation of the CRAB trace in figure 6 follows the temporal evolution of the vector potential, $\mathbf{A}(t)$, of the streaking pulse. The temporal characteristics of the attosecond pulses
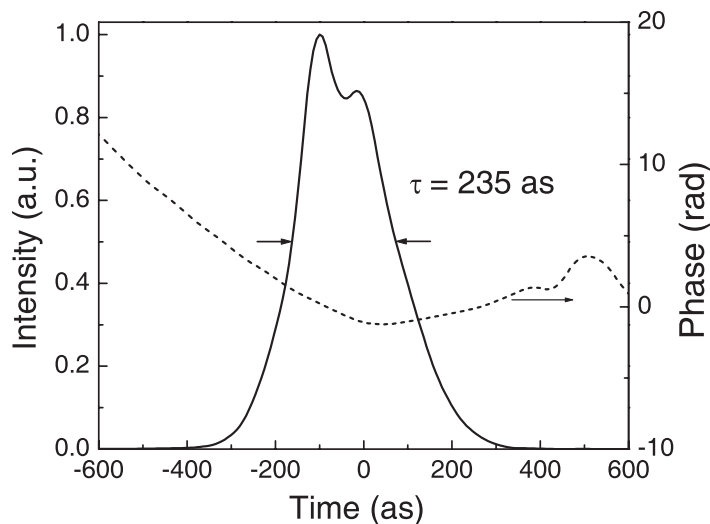
Figure 7. Reconstruction of temporal intensity profile and phase of the attosecond pulses obtained from the CRAB trace shown in figure 6 after 5×10^4 iterations of the PCGPA algorithm. A 100 nm thick Al filter has been used to block the fundamental radiation.

were retrieved using the principal-component generalized projection algorithm (PCGPA) [28]. In the reconstructed temporal intensity profile and phase of the attosecond pulses, reported in figure 7), the pulse duration was 235 as (the Fourier limit is ∼100 as), and the almost parabolic phase indicates the presence of a predominant second-order dispersion, corresponding to a positive linear chirp $C \simeq 33 \, \text{fs}^{-2}$. Such pulses correspond to only 2 optical cycles of the carrier frequency.

It is well known that attosecond pulses are characterized by an intrinsic chirp (atto chirp), due to the fact that the harmonic emission time varies quasi-linearly with harmonic frequency [29]. In particular, the XUV pulses corresponding to the short electron quantum paths present a positive chirp (the spectral components at higher frequencies are emitted after those at lower frequencies) [14]. In order to achieve almost Fourier-transform limited attosecond pulses, it is required to use suitable broad-band chirp compensation techniques. A simple way to compensate for the positive atto chirp is based on the use of x-ray filters with a negative group delay dispersion (GDD) in the spectral region of interest. Negative GDD is provided by Al filters in the energy range from 20 to 60 eV, by silicon filters in the range from 25 to 90 eV and by zirconium filters in the range from 70 to 160 eV [7]. This technique, proposed by Kim *et al* [30], has been used in the case of attosecond pulse trains [6, 7]. In the case of isolated attosecond pulses, duration as short as 130 as was measured by the authors in 2006 by using a 300 nm Al filter to compensate for the intrinsic positive atto chirp [14]: figure 8 shows the reconstructed temporal intensity profile and phase of such pulses.

5. NASP simulations: atto chirp and CEP of attosecond pulses

Since the FROG CRAB technique is not sensitive to the CEP of the attosecond pulses, we have used the NASP method to investigate the temporal evolution of the electric field of the XUV
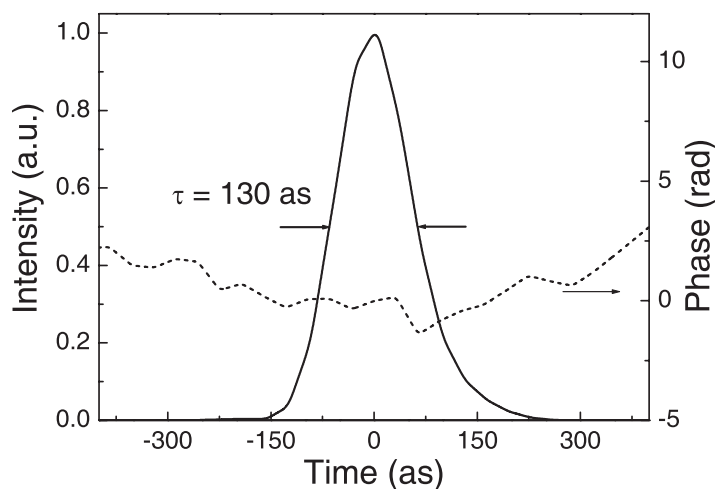
Figure 8. Reconstruction of the temporal intensity profile and phase of the attosecond pulses obtained from the CRAB trace after 5×10^4 iterations of the PCGPA algorithm. A 300 nm thick Al filter has been used to block the fundamental radiation and compensate for the positive atto chirp.
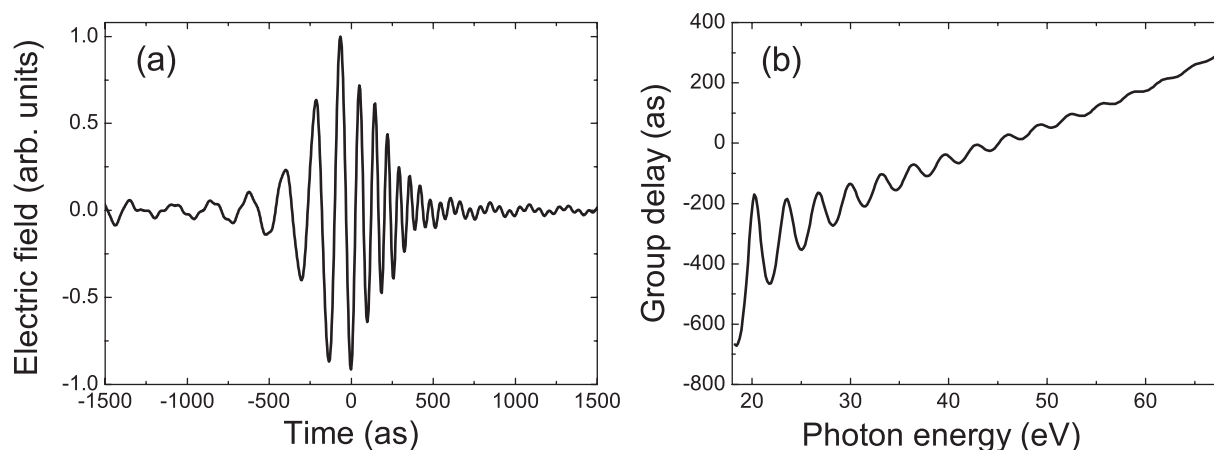

Figure 9. Electric field (a) and group delay (b) of an isolated attosecond pulse, before complete dispersion compensation, generated by 5 fs pulses with modulated polarization state, calculated using the NASP method and assuming the same driving pulse parameters that were used in the experiment.

pulses. In particular, we have analyzed the effects of variations of CEP, intensity and duration of the driving pulses on the XUV field. Figure 9 shows the electric field evolution and the corresponding group delay calculated with the same driving pulse parameters that were used in the experiment without the contribution of the aluminium foil. The pulse, with a duration of 250 as (FWHM of the intensity profile), presents an almost linear and positive chirp. Upon considering the contribution of the aluminium foil, we have calculated a pulse duration of 135 as, in excellent agreement with the experimental result. As pointed out by the authors in [14], the CEP of the XUV pulses turns out to be stable with respect to small changes of the CEP of the driving pulses. Indeed, an IR CEP shift of ~175 mrad has a negligible influence on
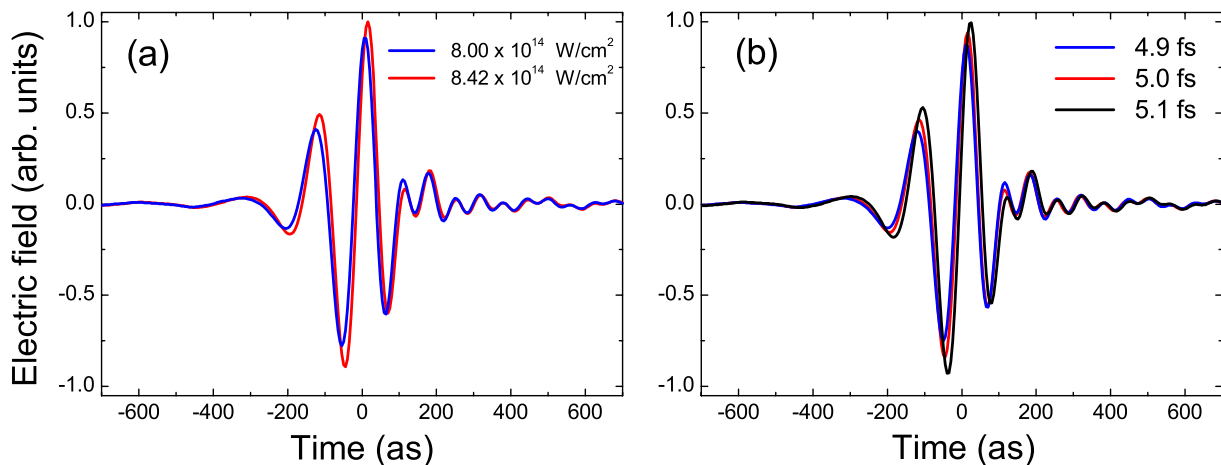
Figure 10. Electric field of ∼135 as isolated pulses calculated by the NASP method for two different values of the driving pulse intensity (a) and for three different driving pulse durations (b). The simulations have been performed assuming the same driving pulse parameters as were used in the experiment.

the CEP of the attosecond pulses. This is particularly important in the applications since the use of a double-feedback active stabilization of the IR pulse CEP allows one to reduce the residual CEP fluctuations to less than 100 mrad. Figure 10(a) shows the effect of a 5% variation of the driving pulse intensity on the XUV electric field: upon changing the driving intensity from $8 \times 10^{14}\,\mathrm{W\,cm^{-2}}$ to $8.42 \times 10^{14}\,\mathrm{W\,cm^{-2}}$ the XUV CEP shifts by ∼350 mrad. Moreover, a variation of the driving pulse duration from 4.9 to 5.1 fs leads to a XUV CEP shift of ∼490 mrad, as shown in figure 10(b). Therefore, the numerical simulations allow one to conclude that the CEP of the near single-cycle attosecond pulses is characterized by remarkable stability.

6. Conclusions

In this work, we have reported on the generation and characterization of spectrally tunable isolated attosecond pulses using the polarization gating method with few-cycle phase stabilized driving pulses. The maximum spectral tuning of the generated XUV radiation is more than 26 eV. The generation of broadband and widely tunable XUV radiation can open a new regime for time-resolved measurements in the attosecond temporal domain. Using numerical simulations based on the NASP method we have analyzed the role of various experimental parameters on the electric field of the few-cycle attosecond pulses.

Acknowledgment

IOP Institute of Physics ⬥ DEUTSCHE PHYSIKALISCHE GESELLSCHAFT

References

[1] Corkum P B and Krausz F 2007 *Nat. Phys.* **3** 381

[2] Scrinzi A, Ivanov M Yu, Kienberger R and Villeneuve D M J 2006 *J. Phys. B: At. Mol. Opt. Phys.* **39** R1

[3] Itatani J, Levesque J, Zeidler D, Niikura H, Pépin H, Kieffer J C, Corkum P B and Villeneuve D M 2004 *Nature* **432** 867

[4] Levesque J and Corkum P B 2006 *Can. J. Phys.* **84** 1

[5] Paul P M, Toma E S, Breger P, Mullot G, Augé F, Balcou Ph, Muller H G and Agostini P 2001 *Science* **292** 1689

[6] López-Martens R *et al* 2005 *Phys. Rev. Lett.* **94** 033001

[7] Gustafsson E, Ruchon T, Swoboda M, Remetter T, Pourtal E, López-Martens R, Balcou Ph and L'Huillier A 2007 *Opt. Lett.* **32** 1353

[8] Hentschel M, Kienberger R, Spielmann Ch, Reider G A, Milosevic N, Brabec T, Corkum P B, Heinzmann U, Drescher M and Krausz F 2001 *Nature* **414** 509

[9] Christov I P, Murnane M M and Kapteyn H 1997 *Phys. Rev. Lett.* **78** 1251

[10] Kienberger R *et al* 2004 *Nature* **427** 817

[11] Corkum P B, Burnett N H and Ivanov M Yu 1994 *Opt. Lett.* **19** 1870

[12] Tckerbakoff O, Mével E, Descamps D, Plumridge J and Constant E 2003 *Phys. Rev.* A **68** 043804

[13] Sola I J *et al* 2006 *Nature Phys.* **2** 319

[14] Sansone G *et al* 2006 *Science* **314** 443

[15] Mairesse Y and Quéré F 2005 *Phys. Rev.* A **71** 011401

[16] Lewenstein M, Balcou Ph, Ivanov M Yu, L'Huillier A and Corkum P B 1994 *Phys. Rev.* A **49** 2117

[17] Sansone G, Vozzi C, Stagira S and Nisoli M 2004 *Phys. Rev.* A **70** 013411

[18] Nisoli M, De Silvestri S and Svelto O 1996 *Appl. Phys. Lett.* **68** 2793

[19] Baltuška A *et al* 2003 *Nature* **421** 611

[20] Caumes J P, Sansone G, Benedetti E, Pascolini M, Poletto L, Villoresi P, Stagira S, Vozzi C and Nisoli M 2006 *J. Mod. Opt.* **53** 67

[21] Yudin G L, Bandrauk A D and Corkum P B 2006 *Phys. Rev. Lett.* **96** 063002

[22] Salières P *et al* 2001 *Science* **292** 902

[23] Milošević D B and Becker W 2002 *Phys. Rev.* A **66** 063417

[24] Kopold R, Milošević D B and Becker W 2000 *Phys. Rev. Lett.* **84** 3831

[25] Walmsley I and Wong V 1996 *J. Opt. Soc. Am.* B **13** 2453

[26] Itatani J, Quéré F, Yudin G L, Ivanov M Yu, Krausz F and Corkum P B 2002 *Phys. Rev. Lett.* **88** 173903

[27] Quéré F, Mairesse Y and Itatani J 2005 *J. Mod. Optics* **52** 339

[28] Kane D 1999 *IEEE J. Quantum Electron.* **35** 421

[29] Mairesse Y *et al* 2003 *Science* **302** 1540

[30] Kim K T, Kim C M, Baik M G, Umesh G and Nam C H 2004 *Phys. Rev.* A **69** 051805